State-Space Integral-Equation Method for the S-Domain Modeling of Planar Circuits on Semiconducting Substrates

Giuseppe Conciauro, *Senior Member, IEEE*, Paolo Arcioni, *Senior Member, IEEE*, and Marco Bressan, *Member, IEEE*

***Abstract*—This paper presents a new and very efficient integral method for the electromagnetic modeling of planar circuits on multilayered semiconducting substrates. Differently from standard integral approaches, the method leads to a state-space model of the circuit. This model directly permits to find the admittance matrix in the form of a reduced-order pole expansion in the S-domain through standard Krylov sub-space techniques. Three examples demonstrate the really good performances of the method in terms of accuracy and rapidity.**

***Index Terms*—Electromagnetic modeling, integral-equation (IE) methods, method of moments, microwave integrated circuits, S-domain methods, state-space methods.**

I. Introduction

PARTICULAR attention is currently devoted to the development of efficient electromagnetic solvers that directly lead to the mathematical model of passive components or subsystems through the application of the so-called S-domain methods [1]. The mathematical model is obtained in the form of pole expansion of some circuit matrix (scattering, impedance, admittance, ...) in the domain of the Laplace variable s. Such models are very useful for representing passive components or subsystems in the design of complex integrated systems, carried out in a network-oriented simulation environment. Furthermore, they can be used to determine almost instantaneously the frequency response with unlimited frequency resolution.

The basic problem encountered in S-domain methods is derived from the necessity of representing a distributed structure, inherently of infinite order, by a macromodel of finite and reasonably small order. Among the many possible techniques suitable for this purpose, the most robust and effective are based on the Krylov sub-space methods, such as the matrix-Padè-via-Lanczos (MPVL) and the block Arnoldi algorithms, largely used in the reduced-order modeling of complex very large scale integration (VLSI) circuitry [2]–[4].

Krylov sub-space methods apply to state-space models of linear systems and, for this reason, they are well-matched to the finite-element method, which gives rise to a model of this type [1], [5], [6]. On the contrary, integral-equation (IE) methods, which are the most effective in the analysis of planar circuits, do not give rise to equations in the state-space form so that Krylov sub-space methods can be applied only through adaptive procedures [7], which partially reduce their efficiency.

In this paper, which presents in detail a theory outlined in [8], we introduce a State-Space Integral-Equation (SS-IE) method for the modeling of shielded planar circuits on multilayered substrates, including semiconductors. Differently from standard IE methods, the new procedure directly results into state equations, thus permitting to exploit at best the advantages of the integral approach and of Krylov sub-space methods. Some preliminary conference papers have been published [9]–[11], which presented a similar method, but restricted to low-loss substrates and lossless metallizations. With respect to the early ones, the algorithm presented here has been modified in order to have real rather than complex system matrices, thus allowing the use of standard model-order reduction techniques. Furthermore, it has been generalized in such a way as to allow for considering lossy substrates and metallizations. With respect to [8], a more accurate representation of the metallization losses has been introduced, an approximate procedure useful in case of low-loss substrates has been included, and the possibility of considering thin-film resistors has been discussed.

Starting from the conventional formulation of the IE method for the analysis of shielded planar circuits, Section II shows how the original equations can be transformed into a state-space model of the circuit. Section III introduces an approximate model useful for speeding up the calculation in the case of high-resistivity semiconductor layers. Section IV suggests how the algorithm can be generalized in order to allow for including thin-film resistors. Section V presents three examples and Section VI draws conclusions.

II. Theory

We consider a shielded planar circuit with N ports, consisting of thin metal elements, embedded in a layered medium including both insulating and semiconducting layers (Fig. 1). For simplicity, we assume that these elements are located at a single "metallization level" outside the semiconducting layers. As usual, we assume a "delta-gap voltage excitation" [12], [13].

The shadowed area Ω shown in Fig. 2 represents the metallization and includes the gaps $t_1, t_2, \ldots, t_N$ where the exciting voltages $v_1, v_2, \ldots, v_N$ are applied. The excitation gives rise to a surface current $\vec{J}$ distributed in the metallization, and to a set

Manuscript received April 16, 2003. This work was supported in part by the Ministero dell'Istruzione, Università e Ricerca under Contract COFIN 2002091132 and Contract FIRB RBNE01NPT9, and by the University of Pavia under Grant FAR 2001-02.

The authors are with the Department of Electronics, University of Pavia, I-27100 Pavia, Italy.

Digital Object Identifier 10.1109/TMTT.2003.819767

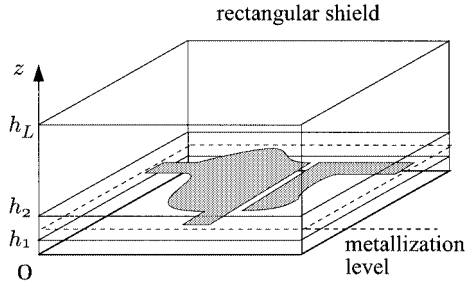

Fig. 1. Shielded planar circuit on a multilayered substrate.

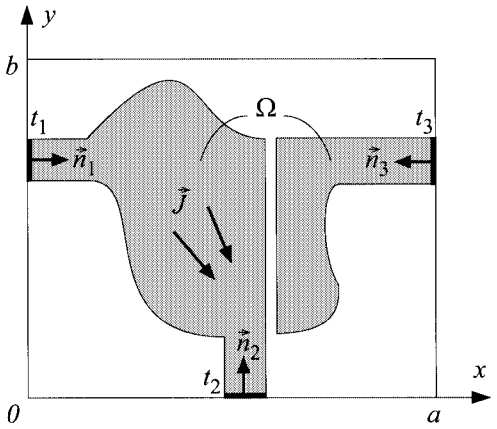

Fig. 2. Symbol definition. The region Ω includes the metallization (shadowed area) and delta gaps (segments $t_1, t_2, \ldots$).

of gap currents $i_1, i_2, \ldots, i_N$. The positive direction of the gap voltages and currents is defined by the normals $\vec{n}_1, \vec{n}_2, \ldots, \vec{n}_N$. We have

$$i_n = \int_{t_n} \vec{J} \cdot \vec{n}_n dt_n \tag{1}$$

Over the surface Ω, the tangential electric field must satisfy the boundary condition

$$\vec{E}_T(x,y) = -\sum_{n=1}^{N} v_n \delta_n \vec{n}_n + Z\vec{J}(x,y) \qquad \forall x,y \in \Omega \tag{2}$$

where δ_n denotes a delta-function supported by the segment t_n, and Z is the surface impedance of the metallization. On the other hand, the electric field is related to the current density by the integral

$$\vec{E}_T(x,y) = -\int_0^a \int_0^b \overline{\overline{Z}}(x,y,x',y') \cdot \vec{J}(x',y')dx'dy' \tag{3}$$

where the Green's dyadic is represented as

$$\overline{\overline{Z}} = \sum_i \mathcal{Z}_i \vec{e}_i(x,y)\vec{e}_i(x'y'). \tag{4}$$

In this expression, vectors $\vec{e}_i$ are the normalized electric mode vectors of the modes of the rectangular waveguide of sides a and b (see Table I), and $\mathcal{Z}_i$ is the modal impedance seen from the metallization level, looking in the layered rectangular cavity. Depending on the mode ordering, the index i corresponds to some TM_{pq} or TE_{pq} mode. For each mode, $\mathcal{Z}_i$ is calculated by considering the transverse equivalent circuit shown in Fig. 3, where each line section corresponds to a layer and the impedances Z_b and Z_t represent the surface impedances of the bottom and top walls of the box, respectively. The propagation factor $(\kappa_i^{(\ell)})$ and the characteristic impedance $(\zeta_i^{(\ell)})$ depend on the layer and on the mode. Their expressions in terms of the Laplace variable s are given in Table I, where σ_ℓ and ϵ_ℓ are the conductivity and the relative permittivity of the ℓth layer and

$$k_i = \sqrt{\left(\frac{p\pi}{a}\right)^2 + \left(\frac{q\pi}{b}\right)^2}, \qquad i \mapsto p,q$$

is the cutoff wavenumber of the mode. The expressions of $\kappa_i^{(\ell)}$ and $\zeta_i^{(\ell)}$ have been obtained by replacing $j\omega$ with s in the usual time–harmonic expressions. On substitution of (3) into (2), we obtain an IE, whose solution yields the current density generated by a given set of voltages. Substituting into (1), we then find the relationship between the voltages and the currents, i.e., the admittance matrix of the circuit. A deembedding procedure (not discussed in this paper) should be applied to correct the results for the effects of parasitics inherent in the "delta-gap" model of the ports.

A. Discretization

The IE is solved by using the method of moments [14]. We approximate the current density in a finite-dimensional functional space using the expression

$$\vec{J} = \sum_{k=1}^{K} c_k \vec{w}_k(x,y) \tag{5}$$

where $\{\vec{w}_k\}$ is a set of real basis functions defined on Ω and $\{c_k\}$ is a set of complex variables. Since, at zero frequency, the current must be solenoidal, the space spanned by $\{\vec{w}_k\}$ must include a subspace of adequate dimensions, consisting of solenoidal functions. Following the Galerkin's procedure, the IE is transformed into the matrix equation

$$\mathbf{Zc} = \mathbf{Tv} \tag{6}$$

where $\mathbf{v} \in \mathcal{C}^N$ is the voltage vector, $\mathbf{c} \in \mathcal{C}^K$ is the vector of the variables c_k, and the matrices $\mathbf{Z} \in \mathcal{C}^{K\times K}$, and $\mathbf{T} \in \Re^{K\times N}$ are defined as

$$Z_{hk} = \sum_i w_{hi} w_{ki} \mathcal{Z}_i + ZK_{hk} \tag{7}$$

$$T_{hn} = \int_{t_n} \vec{w}_h \cdot \vec{n}_n dt_n \tag{8}$$

where

$$w_{hi} = \int_\Omega \vec{w}_h \cdot \vec{e}_i d\Omega \tag{9}$$

$$K_{hk} = \int_\Omega \vec{w}_h \cdot \vec{w}_k d\Omega. \tag{10}$$

TABLE I
PROPAGATION FACTOR, CHARACTERISTIC IMPEDANCES, AND MODE VECTORS

i-th mode	$\kappa_i^{(\ell)}$	$\zeta_i^{(\ell)}$	$\vec{e}_i$
TM_{pq}	$\sqrt{-(s^2\epsilon_0\epsilon_\ell + s\sigma_\ell)\mu_o - k_i^2}$	$\dfrac{j\kappa_i^{(\ell)}}{s\epsilon_0\epsilon_\ell + \sigma_\ell}$	$\sqrt{\dfrac{4ab}{(pb)^2+(qa)^2}}\left(\vec{u}_x\dfrac{p}{a}\cos\dfrac{p\pi x}{a}\sin\dfrac{q\pi y}{b} + \vec{u}_y\dfrac{q}{b}\sin\dfrac{p\pi x}{a}\cos\dfrac{q\pi y}{b}\right)$
TE_{pq}		$\dfrac{s\mu_o}{j\kappa_i^{(\ell)}}$	$\sqrt{\dfrac{2(2-\delta_{p0}-\delta_{q0})ab}{(pb)^2+(qa)^2}}\left(\vec{u}_x\dfrac{p}{b}\cos\dfrac{p\pi x}{a}\sin\dfrac{q\pi y}{b} - \vec{u}_y\dfrac{q}{a}\sin\dfrac{p\pi x}{a}\cos\dfrac{q\pi y}{b}\right)$

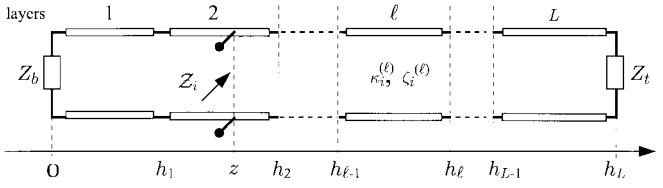

Fig. 3. Equivalent circuit for the calculation of $\mathcal{Z}_i$. The line sections correspond to the layers and z is the metallization level.

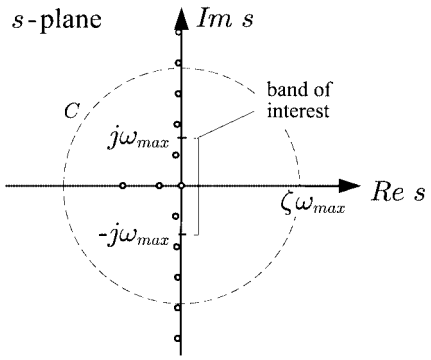

Fig. 4. Typical pole pattern of $\mathcal{Z}_i$ for a TM mode. The accuracy of the approximation (15) increases with increasing the value of the "accuracy factor" ζ. A value ζ of approximately 2–3 is appropriate.

On the other hand, from (1) and (5), we obtain

$$\mathbf{i} = \mathbf{T}^T\mathbf{c} \tag{11}$$

where $\mathbf{i} \in \mathcal{C}^N$ is the current vector. Eliminating $\mathbf{c}$ between (6) and (11), we can find the currents as functions of voltages, i.e., the admittance matrix of the circuit.

B. Pole Expansion of $\mathbf{Z}$

Matrix $\mathbf{Z}$ is a transcendental function of s due to its dependence on the modal and surface impedances. To put (6) into the form of a state equation, we need the pole expansion of $\mathbf{Z}$, which, in turn, requires the introduction of the pole expansions of $\mathcal{Z}_i$ and Z.

The pole expansion of $\mathcal{Z}_i$ can be deduced from the general theory presented in [15], applied to the simple case of isotropic layers, characterized by the constants ϵ_ℓ and σ_ℓ, and assuming that the metallization level is outside the semiconductors. In this case, the expansion has the form

$$\mathcal{Z}_i = \frac{\mathcal{S}_i}{s} + \sum_{\nu=1}^{M_i}\frac{\beta_{i\nu}^2}{s+g_{i\nu}} + \sum_{\mu=1}^{\infty}\left(\frac{\left(\alpha'_{i\mu}+j\alpha''_{i\mu}\right)^2}{s+r_{i\mu}-j\omega_{i\mu}} + \frac{\left(\alpha'_{i\mu}-j\alpha''_{i\mu}\right)^2}{s+r_{i\mu}+j\omega_{i\mu}}\right) \tag{12}$$

where $-g_{i\nu}$ and $(\beta_{i\nu})^2$ represent a real pole and its real residue, $-r_{i\mu}\pm j\omega_{i\mu}$ and $(\alpha'_{i\mu}\pm j\alpha''_{i\mu})^2$ represent a complex pole pair and their residues, the indexes μ and ν label the poles in the order of their increasing distances from the origin, and $\mathcal{S}_i$ is the residue of the pole at the origin. In the particular case where the metallization level is placed just at an insulator/semiconductor interface, this pole does not exist ($\mathcal{S}_i = 0$). Otherwise it exists only for TM modes, and $\mathcal{S}_i$ is real positive.

In the time domain, complex poles correspond to damped oscillating modes of the equivalent circuit of Fig. 3, whereas real poles correspond to damped nonoscillating modes. All poles and residues can be deduced by calculating the eigenmodes of the equivalent circuit [9]. In all cases, we have an infinity of complex poles (with a single cluster point at infinity) and a finite number (M_i) of real poles, as sketched in Fig. 4.

In the case of TM modes, it is found that, with increasing the order i of the mode, and from some order on, M_i tends to a limit (M_∞) that is equal to the number of the interfaces involving at least one semiconducting layer. This result is illustrated in Figs. 5 and 6, which represent the real poles for TM modes versus the cutoff wavenumber in two examples of stratification. The asymptotic values of $g_{i\nu}$ are given by (see Appendix I)

$$g_\infty^{(\ell,\ell+1)} = \frac{\sigma_\ell + \sigma_{\ell+1}}{\epsilon_0(\epsilon_\ell + \epsilon_{\ell+1})}, \qquad \sigma_\ell + \sigma_{\ell+1} \neq 0. \tag{13}$$

In the case of Fig. 5 (low-conductivity layers), the number of real poles is the same for all modes, whereas in the case of Fig. 6 (high-conductivity layer), it decreases when increasing the mode order. A different behavior is found for real poles of TE modes: in fact, these poles either are totally absent or they disappear from some order on. For both types of modes, M_i is a constant (M_∞ or zero) when the conductivity and/or the thickness of semiconducting layers are below some limit (see Section V), beyond which the D-shaped curves of Fig. 6 appear.

An appropriate pole expansion for the surface impedance of the metallization is (see Appendix II)

$$Z = R^{\mathrm{DC}} + s\sum_{m=1}^{\infty}\frac{2R^{\mathrm{DC}}}{s+p_m} \tag{14}$$

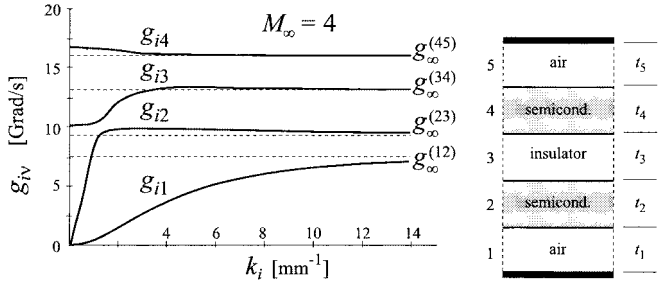

Fig. 5. Real poles versus TM-mode cutoff wavenumber (case of a low-loss structure including dielectric and high-resistivity semiconductor layers). Layer 1 (air): $t_1 = 300\ \mu$m, Layer 2: $t_2 = 100\ \mu$m, $\epsilon_2 = 11$, $\sigma_2 = 10^{-3}$ S/mm. Layer 3: $t_3 = 200\ \mu$m, $\epsilon_3 = 4$, $\sigma_3 = 0$. Layer 4: $t_4 = 400\ \mu$m, $\epsilon_4 = 13$, $\sigma_4 = 2 \cdot 10^{-3}$S/mm. Layer 5 (air): $t_5 = 500\ \mu$m.

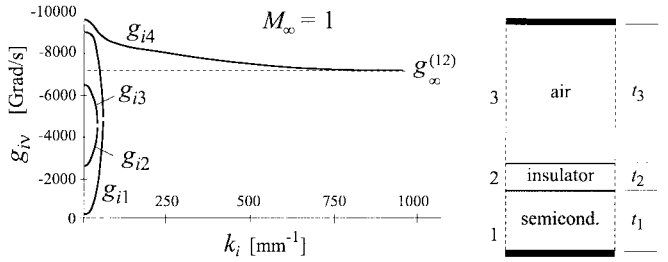

Fig. 6. Real poles versus TM-mode cutoff wavenumber (case of a structure including a low-resistivity substrate and an insulating layer). Layer 1: $t_1 = 100\ \mu$m, $\epsilon_1 = 11.76$, $\sigma_1 = 1$ S/mm. Layer 2: $t_2 = 2\ \mu$m, $\epsilon_2 = 4$, $\sigma_2 = 0$. Layer 3 (air): $t_3 = 1$ mm.

where

$$R^{\mathrm{DC}} = \frac{1}{\sigma_{\mathrm{met}} t} \quad p_m = \frac{\pi^2 m^2}{\mu_{\mathrm{met}} \sigma_{\mathrm{met}} t^2}$$

t, σ_{met}, and μ_{met} representing the actual thickness, conductivity, and magnetic permeability of the metallization, respectively.

Introducing (12) and (14) into (7), we obtain the pole expansion of the matrix $\mathbf{Z}$. Evidently, all the matrix elements have the same poles. More specifically, they have: i) an infinity of complex poles, corresponding to all TE and TM oscillating modes of the box; ii) an infinity of real poles deriving from (14); and iii) a number of real poles $-g_{i\nu}$. Should we consider an infinite number of modes in the expansion (7), also the number of these last poles would be infinite, and they would exhibit M_∞ cluster points, given by (13).

Assuming that an accurate modeling is only required in some given "band of interest" ($-\omega_{\max}$, $\omega_{\max}$), we can approximate in some way the contribution of all poles far from the corresponding portion of the imaginary axis (see Fig. 4). Considering a circle C of radius $\zeta\omega_{\max}$, sufficiently larger than $\omega_{\max}$, we can then truncate the pole expansions (12) by retaining the poles located inside C and approximating the contribution of all other poles by a power expansion around the origin, truncated to the first order. Equation (12) is then replaced by the finite expansion

$$\mathcal{Z}_i \approx \mathcal{R}_i + s\mathcal{L}_i + \frac{\mathcal{S}_i}{s} + \sum_C \frac{\beta_{i\nu}^2}{s + g_{i\nu}} + \sum_C \left(\frac{\left(\alpha'_{i\mu} + j\alpha''_{i\mu}\right)^2}{s + r_{i\mu} - j\omega_{i\mu}} + \frac{\left(\alpha'_{i\mu} - j\alpha''_{i\mu}\right)^2}{s + r_{i\mu} + j\omega_{i\mu}} \right) \quad (15)$$

where Σ_C denotes a summation including only the poles located in C, and $\mathcal{R}_i$ and $\mathcal{L}_i$ are real quantities, such that $\mathcal{R}_i + s\mathcal{L}_i$ approximates the contribution from all poles outside C. All coefficients included in the expansion depend only on the box and metallization level, and can be determined once for all, and used for considering different metallization patterns embedded in the same box. An efficient code for their calculation is described in [9] and can be downloaded from the World Wide Web.[1]

The same criterion can be followed to truncate (14), which can be replaced by the finite expansion (see Appendix II)

$$Z \approx R^{\mathrm{DC}} + sL^{\mathrm{DC}} - s^2 \sum_{m=1}^{M} \frac{z_m^2}{s + p_m} \quad (16)$$

where

$$L^{\mathrm{DC}} = \frac{\mu_{\mathrm{met}} t}{3} \quad z_m = \frac{\sqrt{2\mu_{\mathrm{met}} t}}{\pi m}$$

and M is the number of poles of Z included in C. It is easily verified that

$$M = \mathrm{int}\left(\frac{\sqrt{2\zeta}}{\pi} \frac{t}{\delta} \right) \quad (17)$$

where δ is the skin depth at the frequency $\omega_{\max}$.

Let M' and M'' denote the total number of complex pole pairs and of real poles of the modal impedances included in C, respectively. Due to (7), the pole-set of the matrix $\mathbf{Z}$ then consists of M' complex pole pairs and of $M + M''$ real poles. It is important to note that, with increasing the mode order i, the complex poles of the impedances $\mathcal{Z}_i$ move toward infinity and go outside the circle C. Thus, in all cases, M' is finite (and reasonably small), however large the number of terms included in the summation (7) is. The same statement does not hold true for real poles of the modal impedances because they move toward the asymptotic values (13). If these values are placed inside the circle C (which is likely to happen in the case of high-resistivity semiconductor layers), the number M'' increases with increasing the number of terms included in the summation, and it can be very large. Finally, we note that with the thickness of metallization normally used in monolithic microwave integrated circuits (MMICs), M is of the order of unity.

The poles and residues of the modal impedances are renamed by using a single-index notation with $m' = 1, 2, \ldots, M'$ used for the complex poles and $m'' = 1, 2, \ldots, M''$ used for the real ones. The renaming results into two mappings between the single- and the double-index notations

$$m' \mapsto i, \mu \text{ such that: } \begin{cases} r_{m'} = r_{i\mu} \\ \omega_{m'} = \omega_{i\mu} \\ \alpha'_{m'} = \alpha'_{i\mu} \\ \alpha''_{m'} = \alpha''_{i\mu} \\ w_{hm'} = w_{hi} \end{cases} \quad (18)$$

$$m'' \mapsto i, \nu \text{ such that: } \begin{cases} g_{m''} = g_{i\nu} \\ \beta_{m''} = \beta_{i\nu} \\ w_{hm''} = w_{hi}. \end{cases} \quad (19)$$

[1][Online]. Available: http://www.microwave.unipv.it/software

Summing the two fractions in the last term of (15) and substituting (15) and (16) into (7), we can then write

$$\begin{aligned} Z_{hk} = & R_{hk} + sL_{hk} + \frac{S_{hk}}{s} \\ & + \sum_{m''=1}^{M''} \frac{B_{hm''}B_{km''}\mathrm{sign}\beta_{m''}^2}{s+g_{m''}} - s^2K_{hk}\sum_{m=1}^{M}\frac{z_m^2}{s+p_m} \\ & + \sum_{m'=1}^{M'} A'_{hm'}\frac{(s+r_{m'})A'_{km'} - \omega_{m'}A''_{km'}}{(s+r_{m'})^2+\omega_{m'}^2} \\ & + \sum_{m'=1}^{M'} A''_{hm'}\frac{-(s+r_{m'})A''_{km'} - \omega_{m'}A'_{km'}}{(s+r_{m'})^2+\omega_{m'}^2} \end{aligned} \tag{20}$$

where

$$R_{hk} = \sum_i w_{hi}w_{ki}\mathcal{R}_i + R^{\mathrm{DC}}K_{hk} \tag{21}$$

$$L_{hk} = \sum_i w_{hi}w_{ki}\mathcal{L}_i + L^{\mathrm{DC}}K_{hk} \tag{22}$$

$$S_{hk} = \sum_i w_{hi}w_{ki}\mathcal{S}_i \tag{23}$$

$$A'_{hm'} = \sqrt{2}w_{hm'}\alpha'_{m'} \tag{24}$$

$$A''_{hm'} = \sqrt{2}w_{hm'}\alpha''_{m'} \tag{25}$$

$$B_{hm''} = w_{hm''}|\beta_{m''}|. \tag{26}$$

Note that $S_{hk} = 0$ if the metallization level is placed at a semiconductor/insulator interface because all coefficients $\mathcal{S}_i$ are zero in this case.

C. State-Space Equations and Pole Expansion of the Admittance Matrix

Introducing the auxiliary variables

$$a'_{m'} = \sum_{k=1}^{K}\frac{(s+r_{m'})A'_{km'} - \omega_{m'}A''_{km'}}{(s+r_{m'})^2+\omega_{m'}^2}c_k \tag{27}$$

$$a''_{m'} = \sum_{k=1}^{K}\frac{-(s+r_{m'})A''_{km'} - \omega_{m'}A'_{km'}}{(s+r_{m'})^2+\omega_{m'}^2}c_k \tag{28}$$

$$b_{m''} = \frac{\mathrm{sign}\beta_{m''}^2}{s+g_{m''}}\sum_{k=1}^{K}B_{km''}c_k \tag{29}$$

$$e_k^{(m)} = \frac{sz_m}{s+p_m}c_k \tag{30}$$

and using the pole expansion of $\mathbf{Z}$, (6) becomes

$$\begin{aligned} (\mathbf{R}+s\mathbf{L})\mathbf{c} + s^{-1}\mathbf{S}\mathbf{c} + \mathbf{B}\mathbf{b} - s\mathbf{K}\left(z_1\mathbf{e}^{(1)} + \cdots + z_M\mathbf{e}^{(M)}\right) \\ + \mathbf{A}'\mathbf{a}' + \mathbf{A}''\mathbf{a}'' = \mathbf{T}\mathbf{v} \end{aligned} \tag{31}$$

where the auxiliary variables are ordered in the complex vectors

$$\mathbf{a}', \mathbf{a}'' \in \mathcal{C}^{M'} \quad \mathbf{b} \in \mathcal{C}^{M''} \quad \mathbf{e}^{(m)} \in \mathcal{C}^{K}$$

and the other matrices are defined by (10) and (21)–(26). $\mathbf{R}$, $\mathbf{K}$, $\mathbf{L}$, $\mathbf{S} \in \Re^{K\times K}$ are real square symmetric matrices; $\mathbf{A}'$, $\mathbf{A}'' \in \Re^{K\times M'}$, and $\mathbf{B} \in \Re^{K\times M''}$ are real rectangular matrices.

Matrix $\mathbf{S}$ (if it differs from zero) is semidefinite positive of rank $K' = K - K''$, where K'' is the dimension of the solenoidal subspace spanned by the K-dimensional basis $\{\vec{w}_k\}$ (see Appendix III). It can be expressed in the form of the singular value decomposition (SVD) expansion [16], [17], which, due to the symmetry and positive semidefiniteness, has the form

$$\mathbf{S} = \mathbf{U}\mathbf{\Sigma}\mathbf{U}^T, \qquad \mathbf{U} \in \Re^{K\times K'}; \quad \mathbf{\Sigma} \in \Re^{K'\times K'} \tag{32}$$

where $\mathbf{\Sigma}$ is the (diagonal) matrix of the singular values. Equation (31) can then be modified by substituting

$$s^{-1}\mathbf{S}\mathbf{c} = \mathbf{U}\mathbf{\Sigma}^{\frac{1}{2}}\mathbf{d} \tag{33}$$

where

$$\mathbf{d} = s^{-1}\mathbf{\Sigma}^{\frac{1}{2}}\mathbf{U}^T\mathbf{c}. \tag{34}$$

Starting from (27) and (28), it is easily verified that $a'_{m'}$ and $a''_{m'}$ satisfy

$$(s+r_{m'})a'_{m'} - \omega_{m'}a''_{m'} - \sum_{k=1}^{K}A'_{km'}c_k = 0 \tag{35}$$

$$\omega_{m'}a'_{m'} + (s+r_{m'})a''_{m'} + \sum_{k=1}^{K}A''_{km'}c_k = 0 \tag{36}$$

Furthermore, from (29) and (30), we obtain

$$\mathrm{sign}\beta_{m''}^2(s+g_{m''})b_{m''} - \sum_{k=1}^{K}B_{km''}c_k = 0 \tag{37}$$

$$sz_mc_k - (s+p_m)e_k^{(m)} = 0. \tag{38}$$

Equations (34)–(38) imply the matrix equations

$$(\mathbf{D}' + s\mathbf{I}_{M'})\mathbf{a}' - \mathbf{D}\mathbf{a}'' - \mathbf{A}'^T\mathbf{c} = 0 \tag{39}$$

$$(\mathbf{D}' + s\mathbf{I}_{M'})\mathbf{a}'' + \mathbf{D}\mathbf{a}' + \mathbf{A}''^T\mathbf{c} = 0 \tag{40}$$

$$\left(\mathbf{D}''\mathbf{I}_{M''}^{\pm} + s\mathbf{I}_{M''}^{\pm}\right)\mathbf{b} - \mathbf{B}^T\mathbf{c} = 0 \tag{41}$$

$$s\mathbf{I}_{K'}\mathbf{d} - \mathbf{\Sigma}^{\frac{1}{2}}\mathbf{U}^T\mathbf{c} = 0 \tag{42}$$

$$sz_1\mathbf{K}\mathbf{c} - (s+p_1)\mathbf{K}\mathbf{e}^{(1)} = 0 \tag{43}$$

$$\cdots\cdots\cdots\cdots\cdots$$

$$sz_M\mathbf{K}\mathbf{c} - (s+p_M)\mathbf{K}\mathbf{e}^{(M)} = 0 \tag{44}$$

where $\mathbf{D} = \mathrm{diag}\{\omega_1, \ldots, \omega_{M'}\}$, $\mathbf{D}' = \mathrm{diag}\{r_1, \ldots, r_{M'}\}$, $\mathbf{D}'' = \mathrm{diag}\{g_1, \ldots, g_{M''}\}$, $\mathbf{I}_n$ denotes the identity matrix of order n and

$$\mathbf{I}_{M''}^{\pm} = \mathrm{diag}\left\{\mathrm{sign}\beta_1^2, \ldots, \mathrm{sign}\beta_{M''}^2\right\}.$$

It is noted that (43) and (44) imply (38) because $\mathbf{K}$ is nonsingular (see Appendix III).

Equations (31), (39)–(44), and (11) can be rewritten in the form

$$(\mathbf{M} + s\mathbf{N})\mathbf{x} = \mathbf{T}_{en}\mathbf{v} \tag{45}$$

$$\mathbf{i} = \mathbf{T}_{en}^T\mathbf{x} \tag{46}$$

where the matrices $\mathbf{M}, \mathbf{N}, \mathbf{T}_{en}$, and the vector $\mathbf{x}$ are defined at the bottom of the following page. $\mathbf{M}$ and $\mathbf{N}$ are real symmetric matrices independent of s so that system (45) and (46) represents the mathematical model of the circuit in the standard state-space form, with $\mathbf{x}$ representing the state vector. The model order, i.e., the total number of the state variables, is

$$M_{\mathrm{tot}} = 2M' + M'' + (1+M)K + K'.$$

The model is the basic result of the SS-IE method.

In the particular case where the metallization level is placed at a semiconductor/insulator interface (case $\mathbf{S} = \mathbf{0}$), the model is still valid, with the elimination of the fifth row in the definition of $\mathbf{x}$ and $\mathbf{T}_{en}$ and of the fifth row and column in the definition of $\mathbf{M}$ and $\mathbf{N}$.

From (45) and (46), we obtain

$$\mathbf{i} = \underbrace{\mathbf{T}_{en}^{T}(\mathbf{M} + s\mathbf{N})^{-1}\mathbf{T}_{en}}_{\text{admittance matrix}}\mathbf{v}. \tag{47}$$

Evidently, the admittance matrix defined above is symmetric and satisfies the fundamental property $\mathbf{Y}(s^{\star}) = \mathbf{Y}^{\star}(s)$.

As discussed in numerous papers (e.g., [5]), the inverse matrix is easily obtained in the form of a pole expansion by using the eigendecomposition $\mathbf{MN}^{-1} = \mathbf{H}\mathbf{\Lambda}\mathbf{H}^{-1}$, where $\mathbf{\Lambda}$ is the diagonal matrix of the eigenvalues λ_i and $\mathbf{H}$ is the matrix of the eigenvectors. The elements of the admittance matrix are obtained in the form

$$Y_{ij} = \sum_{n=1}^{M_{\text{tot}}} \frac{k_{ij}^{(n)}}{s + \lambda_n} \tag{48}$$

which evidences that the eigenvalues are the poles of the admittance matrix. Note that the pole expansion is an exact representation of the matrix defined in (47) so that the residues satisfy $k_{ij}^{(n)} = k_{ji}^{(n)}$ and, furthermore, the poles and residues are either real or complex, in conjugate pairs.

The number of poles is equal to the order M_{tot} of the SS-IE model (45) and (46). Though it is much smaller than the typical order of models obtained through finite methods [5], [6], it can be large (e.g., thousands), especially due to the possible large values of M'' and K. This makes the eigendecomposition of $\mathbf{MN}^{-1}$ impractical.

For this reason, the original model is approximated in the band of interest by a reduced-order one. Some Krylov sub-space algorithms, such as the MPVL or the block Arnoldi algorithms [2], can be used, choosing the expansion point on the real positive semiaxis (we use $s_0 = \omega_{\max}/2$), in order to preserve the property $\mathbf{Y}(s^{\star}) = \mathbf{Y}^{\star}(s)$.

Krylov sub-space techniques are iterative processes that improve the approximation by subsequent enlargements of the model order, beginning from a value as low as the number of the ports. The iterative process is stopped when the circuit response (deduced from the pole expansion) converges in the band of interest. The final order of the model depends on the

$$\mathbf{M} = \begin{bmatrix} -\mathbf{D}' & \mathbf{D} & \mathbf{0} & \mathbf{A}'^{T} & \mathbf{0} & \mathbf{0} & \dots & \mathbf{0} \\ \mathbf{D} & \mathbf{D}' & \mathbf{0} & \mathbf{A}''^{T} & \mathbf{0} & \mathbf{0} & \dots & \mathbf{0} \\ \mathbf{0} & \mathbf{0} & -\mathbf{D}''\mathbf{I}^{\pm}_{M''} & \mathbf{B}^{T} & \mathbf{0} & \mathbf{0} & \dots & \mathbf{0} \\ \mathbf{A}' & \mathbf{A}'' & \mathbf{B} & \mathbf{R} & \mathbf{U}\mathbf{\Sigma}^{\frac{1}{2}} & \mathbf{0} & \dots & \mathbf{0} \\ \mathbf{0} & \mathbf{0} & \mathbf{0} & \mathbf{\Sigma}^{\frac{1}{2}}\mathbf{U}^{T} & \mathbf{0} & \mathbf{0} & \dots & \mathbf{0} \\ \mathbf{0} & \mathbf{0} & \mathbf{0} & \mathbf{0} & \mathbf{0} & p_1\mathbf{K} & \dots & \mathbf{0} \\ \dots & \dots & \dots & \dots & \dots & \dots & \dots & \dots \\ \mathbf{0} & \mathbf{0} & \mathbf{0} & \mathbf{0} & \mathbf{0} & \mathbf{0} & \dots & p_M\mathbf{K} \end{bmatrix}$$

$$\mathbf{N} = \begin{bmatrix} -\mathbf{I}_{M'} & \mathbf{0} & \mathbf{0} & \mathbf{0} & \mathbf{0} & \mathbf{0} & \dots & \mathbf{0} \\ \mathbf{0} & \mathbf{I}_{M'} & \mathbf{0} & \mathbf{0} & \mathbf{0} & \mathbf{0} & \dots & \mathbf{0} \\ \mathbf{0} & \mathbf{0} & -\mathbf{I}^{\pm}_{M''} & \mathbf{0} & \mathbf{0} & \mathbf{0} & \dots & \mathbf{0} \\ \mathbf{0} & \mathbf{0} & \mathbf{0} & \mathbf{L} & \mathbf{0} & -z_1\mathbf{K} & \dots & -z_M\mathbf{K} \\ \mathbf{0} & \mathbf{0} & \mathbf{0} & \mathbf{0} & -\mathbf{I}_{K'} & \mathbf{0} & \dots & \mathbf{0} \\ \mathbf{0} & \mathbf{0} & \mathbf{0} & -z_1\mathbf{K} & \mathbf{0} & \mathbf{K} & \dots & \mathbf{0} \\ \dots & \dots & \dots & \dots & \dots & \dots & \dots & \dots \\ \mathbf{0} & \mathbf{0} & \mathbf{0} & -z_M\mathbf{K} & \mathbf{0} & \mathbf{0} & \dots & \mathbf{K} \end{bmatrix}$$

$$\mathbf{x} = \begin{bmatrix} \mathbf{a}' \\ \mathbf{a}'' \\ \mathbf{b} \\ \mathbf{c} \\ \mathbf{d} \\ \mathbf{e}^{(1)} \\ \dots \\ \mathbf{e}^{(M)} \end{bmatrix}$$

$$\mathbf{T}_{en} = \begin{bmatrix} \mathbf{0} \\ \mathbf{0} \\ \mathbf{0} \\ \mathbf{T} \\ \mathbf{0} \\ \mathbf{0} \\ \dots \\ \mathbf{0} \end{bmatrix}$$

nature of the component and the band of interest. Also, in cases of high-order filters and very large bands of interest, it does not exceed some tens. The eigendecomposition of matrices of such an order does not give rise to any computing problem.

III. High-Resistivity Layers

MMICs make use of high-resistivity layers with typical conductivity smaller than 0.1 S/m and thickness smaller than a few hundreds of micrometers. In this case, it is found that real poles exist for TM modes only, that their residues $\beta_{i\nu}^2$ are positive, and that their number M_i is equal to the number M_∞ of the asymptotic values (13). Typically, these values are smaller than $2\pi \cdot 10^8$ rad/s, corresponding to frequencies well below the microwave range. For this reason, the poles $-g_1, \ldots, -g_{M''}$ crowd together near to the origin, at distances much smaller than the radius of the circle C.

Due to the mapping (19), indexes m'' always correspond to TM modes, and each TM mode correspond to M_∞ of these indexes. For this reason, we have

$$M'' = M_\infty M^{\mathrm{TM}} \tag{49}$$

where M^{TM} is the number of TM modes considered in the summation (7). Since M^{TM} may easily be of the order of a few thousands, M'' can be very large, giving the largest contribution to the order M_{tot}. Though the model-order reduction permits to also handle cases of thousands of state variables without particular problems, the rapidity of the reduction process is affected by the large dimension of the involved matrices. In this section, we introduce an approximation that eliminates this drawback without loosing accuracy in the microwave range.

Due to (23) and (41) and observing that, in the present case, we have $\mathbf{I}_{M''}^{\pm} = \mathbf{I}_{M''}$ (because $\beta_{m''}^2 > 0$), we can write

$$s^{-1}\mathbf{S}\mathbf{c} + \mathbf{B}\mathbf{b} = \mathbf{W}\mathbf{Q}\Big(\widehat{\mathbf{D}}'' + s\mathbf{I}_{M^{\mathrm{TM}}+M''}\Big)^{-1}\mathbf{Q}\mathbf{W}^T\mathbf{c} \tag{50}$$

where (assuming $\mathbf{S} \neq \mathbf{0}$)

$$\mathbf{W} = [\mathbf{W}' \quad \mathbf{W}''] \quad \widehat{\mathbf{D}}'' = \begin{bmatrix} \mathbf{0} & \mathbf{0} \\ \mathbf{0} & \mathbf{D}'' \end{bmatrix}.$$

In this expression, $\mathbf{W}' \in \Re^{K \times M^{\mathrm{TM}}}$ is the matrix of the quantities w_{hi} pertaining to the TM modes, $\mathbf{W}'' \in \Re^{K \times M''}$ is the matrix of the quantities $w_{hm''}$, $\mathbf{D}''$ is the same matrix defined in the preceding section, and

$$\mathbf{Q} = \mathrm{diag}\left\{S_1^{\frac{1}{2}}, \ldots, S_{M^{\mathrm{TM}}}^{\frac{1}{2}}, \beta_1, \ldots, \beta_{M''}\right\}.$$

It is stressed that, in the present case, the entries $w_{hm''}$ of $\mathbf{W}''$ also pertain to TM modes only, and that each row of $\mathbf{W}'$ appears M_∞ times as a row of $\mathbf{W}''$ in positions depending on the mapping (19). For this reason, the rank of $\mathbf{W}$ is equal to the rank of $\mathbf{W}'$, which, in turn, is equal to the rank (K') of $\mathbf{S}$ (see Appendix III). We can then represent $\mathbf{W}$ by the SVD expansion [16], [17] as follows:

$$\mathbf{W} = \widehat{\mathbf{U}}\widehat{\mathbf{\Sigma}}\mathbf{V}^T$$

where $\widehat{\mathbf{U}} \in \Re^{K \times K'}$, $\mathbf{V} \in \Re^{(M^{\mathrm{TM}}+M'') \times K'}$, and $\widehat{\mathbf{\Sigma}} \in \Re^{K' \times K'}$ is the diagonal matrix of the singular values of $\mathbf{W}$. We can then rewrite (50) in the form

$$s^{-1}\mathbf{S}\mathbf{c} + \mathbf{B}\mathbf{b} = \widehat{\mathbf{U}}\widehat{\mathbf{\Sigma}}\widehat{\mathbf{b}} \tag{51}$$

where

$$\widehat{\mathbf{b}} = \mathbf{V}^T\mathbf{Q}\Big(\widehat{\mathbf{D}}'' + s\mathbf{I}_{M^{\mathrm{TM}}+M''}\Big)^{-1}\mathbf{Q}\mathbf{V}\widehat{\mathbf{\Sigma}}\widehat{\mathbf{U}}^T\mathbf{c}. \tag{52}$$

The nonzero entries of $\widehat{\mathbf{D}}''$, i.e., the real poles of $\mathbf{Z}$ that depend on the losses in the semiconducting layers, are located very near to the origin. If we are not interested in the range of low frequencies, we can then assume that $\widehat{\mathbf{b}}$ satisfies the approximate equation (see Appendix IV)

$$\Big(\mathbf{X}^{-1}\widehat{\mathbf{X}}\mathbf{X}^{-1} + s\mathbf{X}^{-1}\Big)\widehat{\mathbf{b}} - \widehat{\mathbf{\Sigma}}\widehat{\mathbf{U}}^T\mathbf{c} \approx 0, \qquad \text{for } |s| \gg \max\{g_{m''}\} \tag{53}$$

where

$$\mathbf{X} = \mathbf{V}^T\mathbf{Q}^2\mathbf{V} \quad \widehat{\mathbf{X}} = \mathbf{V}^T\mathbf{Q}\widehat{\mathbf{D}}''\mathbf{Q}\mathbf{V} \qquad \mathbf{X}, \widehat{\mathbf{X}} \in \Re^{K' \times K'}. \tag{54}$$

By substituting (51) into (31) and replacing (41) and (42) with (53), we still obtain the state-space model (45) and (46) with the following new definitions of $\mathbf{M}$, $\mathbf{N}$, $\mathbf{T}_{en}$, and $\mathbf{x}$:

$$\mathbf{M} = \begin{bmatrix} -\mathbf{D}' & \mathbf{D} & \mathbf{0} & \mathbf{A}'^T & \mathbf{0} & \ldots & \mathbf{0} \\ \mathbf{D} & \mathbf{D}' & \mathbf{0} & \mathbf{A}''^T & \mathbf{0} & \ldots & \mathbf{0} \\ \mathbf{0} & \mathbf{0} & -\mathbf{X}^{-1}\widehat{\mathbf{X}}\mathbf{X}^{-1} & \widehat{\mathbf{\Sigma}}\widehat{\mathbf{U}}^T & \mathbf{0} & \ldots & \mathbf{0} \\ \mathbf{A}' & \mathbf{A}'' & \widehat{\mathbf{U}}\widehat{\mathbf{\Sigma}} & \mathbf{R} & \mathbf{0} & \ldots & \mathbf{0} \\ \mathbf{0} & \mathbf{0} & \mathbf{0} & \mathbf{0} & p_1\mathbf{K} & \ldots & \mathbf{0} \\ \ldots & \ldots & \ldots & \ldots & \ldots & \ldots & \ldots \\ \mathbf{0} & \mathbf{0} & \mathbf{0} & \mathbf{0} & \mathbf{0} & \ldots & p_M\mathbf{K} \end{bmatrix}$$

$$\mathbf{N} = \begin{bmatrix} -\mathbf{I}_{M'} & \mathbf{0} & \mathbf{0} & \mathbf{0} & \mathbf{0} & \ldots & \mathbf{0} \\ \mathbf{0} & \mathbf{I}_{M'} & \mathbf{0} & \mathbf{0} & \mathbf{0} & \ldots & \mathbf{0} \\ \mathbf{0} & \mathbf{0} & -\mathbf{X}^{-1} & \mathbf{0} & \mathbf{0} & \ldots & \mathbf{0} \\ \mathbf{0} & \mathbf{0} & \mathbf{0} & \mathbf{L} & -z_1\mathbf{K} & \ldots & -z_M\mathbf{K} \\ \mathbf{0} & \mathbf{0} & \mathbf{0} & -z_1\mathbf{K} & \mathbf{K} & \ldots & \mathbf{0} \\ \ldots & \ldots & \ldots & \ldots & \ldots & \ldots & \ldots \\ \mathbf{0} & \mathbf{0} & \mathbf{0} & -z_M\mathbf{K} & \mathbf{0} & \ldots & \mathbf{K} \end{bmatrix}$$

$$\mathbf{x} = \begin{bmatrix} \mathbf{a}' \\ \mathbf{a}'' \\ \widehat{\mathbf{b}} \\ \mathbf{c} \\ \mathbf{e}^{(1)} \\ \ldots \\ \mathbf{e}^{(M)} \end{bmatrix}$$

$$\mathbf{T}_{en} = \begin{bmatrix} \mathbf{0} \\ \mathbf{0} \\ \mathbf{0} \\ \mathbf{T} \\ \mathbf{0} \\ \ldots \\ \mathbf{0} \end{bmatrix}.$$

Since $\widehat{\mathbf{b}}$ is a K'-dimensional vector, the order of the approximate model is

$$\widehat{M}_{\mathrm{tot}} = 2M' + (1+M)K + K' = M_{\mathrm{tot}} - M''.$$

The order of the approximate model is then much smaller than the order of the original one.

The approximate model is still valid in the case $\mathbf{S} = \mathbf{0}$; the only modification consisting in defining $\mathbf{W} = \mathbf{W}''$, $\widehat{\mathbf{D}}'' = \mathbf{D}''$, and $\mathbf{Q} = \mathrm{diag}\{\beta_1, \ldots, \beta_{M''}\}$.

IV. Inclusion of Thin-Film Resistors

The theory discussed in the previous section can be slightly modified to allow for considering metallizations with a piecewise constant (rather than a constant) surface impedance. This permits to consider thin-film resistors connected to the high-conductivity metallization. The modification starts from (7), where the quantity ZK_{hk} must be replaced by $\int Z(x,y)\vec{w}_h \cdot \vec{w}_k d\Omega$. In the subdomain of Ω corresponding to resistors, Z is simply represented by a resistance, independent of s. In the subdomains corresponding to the high-conductivity metallization, Z is still represented by (16). Though the generalization creates no significant conceptual problem, it requires a more complicate definition of matrices related to metal losses. We limited the presentation of the theory to the simplest case of a uniform metallization to avoid overwhelming the basic concepts with a cumbersome symbolism.

V. Examples

In this section, we compare the results of the SS-IE algorithm, implemented in a FORTRAN code, with the results obtained by a commercial code based on the standard IE algorithm (AWR EMSight) with the deembedding procedure disabled. As in EMSight, we used rectangular rooftops as basis functions [18] in such a way as to make the comparison independent of the choice of these functions. Note that rooftops permit to synthesize solenoidal currents [10], thus fulfilling the requirement discussed in Section II-A. The model-order reduction has been performed by using an MPVL algorithm. After determining the pole expansion of the Y-matrix, we calculated the scattering parameters by using well-known transformation formulas. The frequency sweep requires a negligible time. All reported times refer to a standard PC with a 2-GHz Pentium-IV processor and a 512-MB RAM. All times are reported in the form of the sum of two contributions; the first representing the time required for the determination of all the coefficients involved in the representation the modal impedances (15) and the second representing the time required for the calculation of the system matrices, for the model-order reduction and for the eigendecomposition of $\mathbf{MN}^{-1}$.

The first example (Fig. 7) refers to a section (1.2 mm) of a microstrip line on a medium-conductivity Si–SiO_2 substrate, analyzed in the frequency range of 0–20 GHz. The width of the microstrip was chosen to give a characteristic impedance close to 50 Ω at 10 GHz. Due to the conductivity of the substrate, this structure exhibits a slow-wave effect at low frequencies [19]. In the calculation, we deduced the attenuation and the "slowing factor" c/v from the amplitude and phase of S_{21}. In the calculation, we used $K = 63$ rooftops (uniform mesh, 100 μm × 18 μm) and represented the field with an expansion involving 1280 TE modes and 1200 TM modes. The maximum frequency of interest was $f_{\max} = 20$ GHz and we chose $\zeta = 3$. With this choice, we found $M = 1$, $M'' = 1200$, $M' = 0$

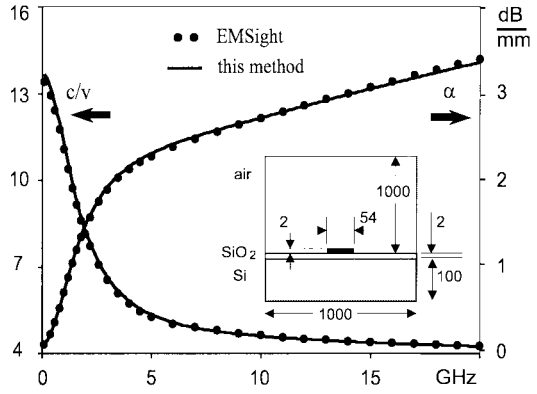

Fig. 7. Slowing factor and attenuation in a microstrip line on a medium-resistivity Si–SiO_2 substrate showing the slow-wave effect at low frequencies. All dimensions are in micrometers (figure not to scale). The stratification data are $\epsilon_1 = 11.76$, $\sigma_1 = 10$ S/m, $\epsilon_2 = 3.9$, and $\sigma_2 = 0$. The conductivity of the strip and the ground plane was 10^7 S/m.

(no complex pole pair were found inside the circle C so that $\mathbf{A}'$, $\mathbf{A}''$, $\mathbf{D}$, $\mathbf{D}'$, $\mathbf{a}'$, and $\mathbf{a}''$ were missing in the calculation). The original model order was $M_{\mathrm{tot}} = 1362$, which was reduced to ten by the MPVL algorithm. The results obtained by the SS-IE and the IE methods are in good agreement (the slowing factor and the attenuation agree within 2% and 0.03 dB/mm, respectively). With our method, the computing time was approximately $(2 + 1)$ s, whereas the time required by EMSight to calculate the 32 frequency samples reported in the figure was approximately 12 s (with the same rooftops). It is noted that, in this example, the accelerated procedure described in Section III could not be used since the value of the largest real pole (of the order of $2\pi \cdot 15$ Grad/s) was comparable with the radius of the circle C.

The structure of Fig. 7 was also used to investigate the behavior of the SS-IE algorithm when the conductivity of the semiconductor is increased, beginning from the value of 10 S/m considered before. At first, the number M'' of real poles inside the circle C decreased, going to zero when the conductivity reached a value for which the asymptotic value (13) exceeded the radius of C. Disappearance of real poles took place for a conductivity of approximately 50 S/m. Real poles appeared again, for lower order TE and TM modes only, for a conductivity of the order of

$$\frac{\pi\sqrt{\epsilon_{\mathrm{sem}}}}{\eta_0 d}$$

where η_0 has the usual meaning and ϵ_{sem}, d are the permittivity and thickness of the semiconductor, respectively. It is noted that this value of conductivity corresponds to the appearance of the D-shaped curves in the diagram $g_{i\nu}$ versus k_i (see Fig. 6). The number M'' reached again the order of 1000 for a conductivity of the order of 10^4 S/m, a very large value, typically encountered only in RF integrated circuits (RFICs), rather than in MMICs. Only when such a value was largely exceeded, the number of real poles increased up to a point that makes the SS-IE algorithm less efficient. Though these results refer to a particular structure, a similar behavior has also been observed for different structures, e.g., in cases where the semiconducting layer does not contact the ground plane.

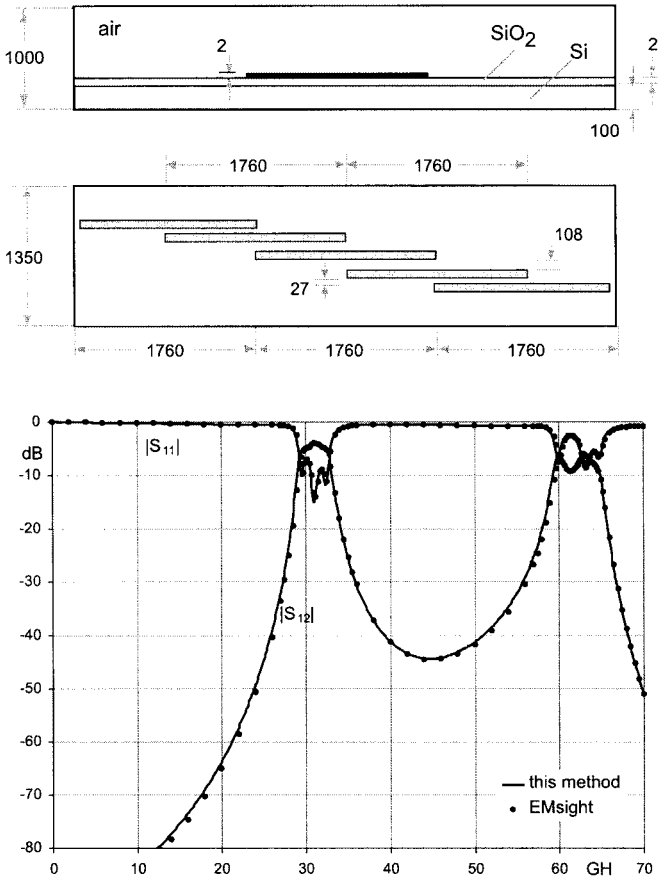

Fig. 8. Coupled-line 30-GHz bandpass filter on an Si–SiO_2 high-resistivity substrate, modeled in a very large band, including the first spurious passband. All dimensions are in micrometers (drawing not to scale). The width of all strips is 81 μm). The stratification data are $\epsilon_1 = 11.76$, $\sigma_1 = 1/30$ S/m, $\epsilon_2 = 3.9$, and $\sigma_2 = 0$. The conductivity of the strip and the ground plane was 10^7 S/m.

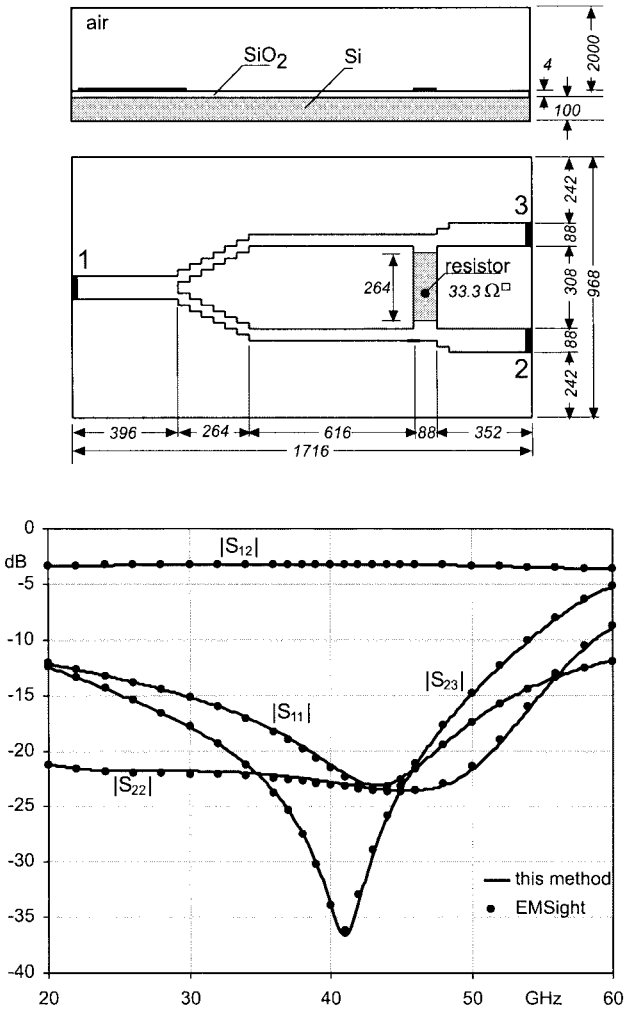

Fig. 9. 40-GHz Wilkinson power divider on a high-resistivity Si–SiO_2 substrate ($\epsilon_1 = 11.76$, $\sigma_1 = 1/30$ S/m, $\epsilon_2 = 3.9$, $\sigma_2 = 0$).

The second example (Fig. 8) concerns a 30-GHz coupled-line bandpass filter on a high-resistivity Si–SiO_2 substrate. This example was already considered in [8], where we assumed $Z = R^{\rm DC}$ for the sake of simplicity. It is reconsidered here to see the effect of the more accurate representation (16). We used $K = 291$ rooftops (uniform mesh, 146.66 μm $\times$ 27 μm) and represented the field with an expansion involving 2805 TE modes and 2700 TM modes. The maximum frequency of interest was $f_{\max} = 70$ GHz (in order to include in the analysis the first spurious passband of the filter) and we chose $\zeta = 3$. With this choice, we found $M = 2$, $M' = 32$, and $M'' = 2700$ and the original model-order was $M_{\rm tot} = 3814$. The MPVL algorithm reduced the order to 80. The computing time was (5+25) s, to be compared with 150 s required by EMSight to compute (with the same rooftops) the 194 frequency samples reported in the figure. An excellent agreement between the SS-IE and IE results is observed (in the passband, the insertion and return loss agree within 0.4 and 0.9 dB, respectively). The time saving became even more important if the accelerated procedure of Section III is used, as permitted due to the high resistivity of the substrate. With this procedure, we had $M_{\rm tot} = 1114$, which was reduced to 60 by the MPVL algorithm. The computing time became (5+12) s, showing the advantage of the accelerated procedure. The results obtained with both procedures are indistinguishable apart from fine details at very low frequencies, not appreciable in Fig. 8. With respect to the result reported in [8, Fig. 5], an increase of insertion loss of approximately 3 dB in the passband and a significant deformation of the response is observed. This result confirms the importance of using an s-dependent rather than a constant value of the surface impedance of the metallization.

The last example refers to a symmetric Wilkinson power divider on a high-resistivity Si–SiO_2 substrate (Fig. 9), which includes a distributed thin-film resistor. In the analysis of this structure, we considered a piecewise constant surface impedance (see Section IV), assuming a lossless metallization for the microstrip lines and a resistance of 33.33 Ω per square for the resistor. We used $K = 472$ rooftops and represented the field with an expansion involving 7170 TE modes and 7000 TM modes. The maximum frequency of interest was $f_{\max} = 60$ GHz and we chose $\zeta = 3$. With this choice, we found $M' = 4$ and $M'' = 7000$. Note that, in this example, we had $M = 0$ due to the assumption of an infinite conductivity in the strip lines. Also in this case, we used the accelerated procedure of Section III, which resulted in the model-order $M_{\rm tot} = 773$ reduced to 30 after using the MPVL algorithm.

Again, a very good agreement between the SS-IE and IE results is observed (typically within 0.15 dB). With our method, the computing time was approximately (12+11) s, whereas EM-Sight required approximately 70 s to compute the 26 frequency samples reported in the figure. In this example, nonuniform meshes were used in either simulations. Though different meshing criteria produced slightly different meshes, in both case, the minimum mesh size was 22 μm $\times$ 22 μm.

As in most commercial codes based on the IE approach, also with the SS-IE algorithm, it is possible to reuse previous results to save computing time when repeating calculations with the same layered box and different geometries of the metallization. In fact, the evaluation of the coefficients of the pole expansions (15) can be performed once for all, thus obtaining a time saving of approximately 30%–50%, as shown by the times quoted above.

VI. Conclusions

It has been shown how the IE method can be modified to give place to a state-space model of a shielded planar circuit. The relatively small order of the model permits to perform the model-order reduction in very short times by using a Krylov sub-space technique and avoiding the interpolation procedures used in other S-domain IE methods. Some examples demonstrated the accuracy of the method and the time saving obtainable in the calculation of frequency response in very large bands. Apart from the time saving, the SS-IE method has the advantage of generating in a reliable way mathematical models, which can be very useful for representing arbitrarily shaped planar structures in the design of complex integrated circuits, carried out in a network-oriented simulation environment.

Numerical experiments demonstrated that the efficiency of the SS-IE method is maintained in a very large range of conductivity of the semiconducting layers, including all values of practical interest.

Though the theory has been reported for the simple case of a single metallization level, it can be extended to circuits with multiple metallizations and/or vias. The generalization requires the use of a representation of the electric field involving a nine-component dyadic $\overline{\overline{Z}}(x,y,z,x',y',z')$. The pole expansion of this dyadic can also be obtained from the general results reported in [15], and its use leads to the state-space formulation of the problem, following the same lines discussed here. Some complication could only derive from the representation of the surface impedance of the metal elements.

Appendix I
Asymptotic Values of $g_{i\nu}$

The asymptotic values of the real poles are nonzero and finite. They correspond to damping factors of damped nonoscillating modes of the equivalent circuit of Fig. 3, considered in the limit of very large values of k_i. They can be found as the nonzero and finite "natural values" of s for which, in the absence of external excitation, waves can exist in the equivalent circuit, in the limiting case $k_i \to \infty$.

With increasing the cutoff wavenumber and for finite values of s, we have (see Table I)

$$j\kappa_i^{(\ell)} \to k_i \quad \zeta_i^{(\ell)} \to \begin{cases} \dfrac{k_i}{s\epsilon_0\epsilon_\ell + \sigma_\ell}, & \text{for TM modes} \\ \dfrac{s\mu_0}{k_i}, & \text{for TE modes.} \end{cases} \tag{55}$$

Since $j\kappa_i$ is real and very large, the modes we are considering consist of strongly attenuated evanescent waves. As a consequence, these modes, when they exist, must be localized in the close proximity and on both sides of interfaces between the layers. They correspond to values of s for which the admittances seen on both sides of the interfaces are opposite. On the other hand, these admittances correspond to the characteristic admittances of the adjacent layers since the strong attenuation makes the effect of all other layers negligible. Therefore, the desired values of s are solutions of the equations

$$\frac{1}{\zeta_i^{(\ell)}(s)} = -\frac{1}{\zeta_i^{(\ell+1)}(s)}, \qquad \ell = 1, \ldots, L-1.$$

By substituting (55), we found that no solution exists in the case of TE modes, whereas, in the case of TM modes, we have a nonzero solution for each interface where $\sigma_\ell + \sigma_{\ell+1} \neq 0$, i.e., for each interface involving one semiconducting layer, at least. The solution is

$$s = -\frac{\sigma_\ell + \sigma_{\ell+1}}{\epsilon_0(\epsilon_\ell + \epsilon_{\ell+1})} = -g_\infty^{(\ell,\ell+1)}$$

which corresponds to the asymptotic values (13).

Appendix II
Pole Expansion of Z

An expression of Z appropriate to microstrip circuits is [20]

$$Z = \left(\frac{s\mu_{\rm met}}{\sigma_{\rm met}}\right)^{\frac{1}{2}} \operatorname{cth}\left((s\mu_{\rm met}\sigma_{\rm met})^{\frac{1}{2}}\, t\right). \tag{56}$$

This expression is transformed into (14) by using the expansion (see [21, eq. 1.421.4])

$$\operatorname{cth} x = \frac{1}{x} + 2x \sum_{m=1}^{\infty} \frac{1}{x^2 + m^2\pi^2}.$$

The convergence of (14) is accelerated by extracting from the series its value for $s = 0$, i.e.,

$$\sum_{m=1}^{\infty} \frac{1}{p_m} = \frac{\mu_{\rm met}\sigma_{\rm met}t^2}{\pi^2} \sum_{m=1}^{\infty} \frac{1}{m^2} = \frac{\mu_{\rm met}\sigma_{\rm met}t^2}{\pi^2}\frac{\pi^2}{6}.$$

Thanks to the accelerated convergence, the series is truncated by considering the contribution of the only poles included in the circle C. Thus, we obtain (16), where

$$M = \max\{m\} : p_m = \frac{\pi^2 m^2}{\mu_{\rm met}\sigma_{\rm met}t^2} \leq \zeta\omega_{\max}.$$

From this condition, we obtain (17).

APPENDIX III
SOME PROPERTIES OF $\mathbf{S}$, $\mathbf{K}$, AND $\mathbf{W}'$

Due to (23), a quadratic form depending on $\mathbf{S}$ can be written as

$$\begin{aligned} q_S &= \sum_{h=1}^{K}\sum_{k=1}^{K} c_h^* S_{hk} c_k \\ &= \sum_{i}^{(\mathrm{TM})} \mathcal{S}_i \sum_{h=1}^{K} c_h^* w_{hi} \sum_{k=1}^{K} c_k w_{ki} \\ &= \sum_{i}^{(\mathrm{TM})} \mathcal{S}_i \left| \sum_{k=1}^{K} c_k w_{ki} \right|^2 \end{aligned}$$

where the summation over the modal index i is limited to TM modes only since $S_i = 0$ for TE modes. On the other hand, due to (9), we have

$$\sum_{k=1}^{K} c_k w_{ki} = \int_{\Omega} \vec{e}_i^{\,\mathrm{TM}} \cdot \sum_{k=1}^{K} c_k \vec{w}_k d\Omega = \int_{\Omega} \vec{e}_i^{\,\mathrm{TM}} \cdot \vec{J} d\Omega. \quad (57)$$

The integral can be zero for any $\vec{e}_i^{\,\mathrm{TM}}$ only if $\vec{J}$ is zero or if $\nabla \cdot \vec{J} = 0$ (electric TM-mode vectors are orthogonal to transverse solenoidal vectors). Quanity q_S is then zero only if all c-coefficients are zero or if they correspond to solenoidal currents. In other cases, q_S is positive so that matrix $\mathbf{S}$ is semidefinite positive, and its null space consists of the c vectors that represent solenoidal currents. The dimension of this space is equal to the dimension K'' of the solenoidal subspace spanned by the K-dimensional basis $\{\vec{w}_k\}$. The rank of S is then $K' = K - K''$.

Now let us consider the quadratic form

$$q_K = \sum_{h=1}^{K}\sum_{k=1}^{K} c_h^* K_{hk} c_k.$$

Due to (10) and (5), this expression is easily transformed into

$$q_K = \int_{\Omega} \vec{J}^* \cdot \vec{J} d\Omega$$

which shows that q_K is positive for all $\mathbf{c} \neq 0$. Consequently, $\mathbf{K}$ is nonsingular and positive definite.

Finally, we observe that (57) represents the ith raw of the vector $\mathbf{W}'^T\mathbf{c}$, $\mathbf{W}'$ representing the matrix of coefficients w_{ki} pertaining to TM modes included in the field representation (3) and (4). For this reason, the null space of $\mathbf{W}'^T$ is the same as the null space of $\mathbf{S}$ so that the rank of $\mathbf{W}'$ is the same as the rank K' of $\mathbf{S}$.

APPENDIX IV
APPROXIMATIONS FOR THE CASE OF HIGH-RESISTIVITY LAYERS

If $|s| \gg \max\{g_{m''}\}$, the entries of $s^{-1}\widehat{\mathbf{D}}''$ can be regarded as infinitesimal quantities, and we can write

$$\left(\mathbf{I}_{M^{\mathrm{TM}}+M''} + s^{-1}\widehat{\mathbf{D}}''\right)^{-1} \approx \mathbf{I}_{M^{\mathrm{TM}}+M''} - s^{-1}\widehat{\mathbf{D}}''.$$

Using this approximation and introducing the matrices $\mathbf{X}$ and $\widehat{\mathbf{X}}$, defined in (54), from (52), we obtain

$$s\left(\mathbf{X} - s^{-1}\widehat{\mathbf{X}}\right)^{-1} \approx \widehat{\mathbf{\Sigma}}\widehat{\mathbf{U}}^T\mathbf{c}.$$

Also, $s^{-1}\widehat{\mathbf{X}}$ can be regarded as an infinitesimal matrix. Again making the same kind of approximation, we can then write

$$\begin{aligned} \left(\mathbf{X} - s^{-1}\widehat{\mathbf{X}}\right)^{-1} &= \mathbf{X}^{-1}\left(\mathbf{I}_{K'} - s^{-1}\widehat{\mathbf{X}}\mathbf{X}^{-1}\right)^{-1} \\ &\approx \mathbf{X}^{-1}\left(\mathbf{I}_{K'} + s^{-1}\widehat{\mathbf{X}}\mathbf{X}^{-1}\right). \end{aligned}$$

By substituting in the preceding equation, we then obtain (53).

ACKNOWLEDGMENT

The authors express their gratitude to Prof. V. Simoncini, University of Bologna, Bologna, Italy, and the Istituto di Analisi Numerica–Consiglio Nazionale delle Ricerche (IAN–CNR), Pavia, Italy, for her valuable help and advise in the choice of MPVL routines.

REFERENCES

[1] J. E. Bracken, D. K. Sun, and Z. J. Cendes, "S-domain methods for simultaneous time and frequency characterization of electromagnetic devices," *IEEE Trans. Microwave Theory Tech.*, vol. 46, pp. 1277–1290, Sept. 1998.

[2] R. W. Freund, "Reduced-order modeling techniques based on Krylov subspaces and their use in circuit simulation," Bell Labs., Murray Hill, NJ, Numer. anal. manuscript 98-3-02. [Online]. Available: http://cm.bell-labs.com/cs/doc/98, Feb. 1998.

[3] Z. Bai, P. M. Dewilde, and R. W. Freund, "Reduced-order modeling," Bell Labs., Murray Hill, NJ, Numer. anal. manuscript 02-4-13, [Online]. Available: http://cm.bell-labs.com/cs/doc/02, Mar. 2002.

[4] A. Odabasioglu, M. Celik, and L. P. Pileggi, "PRIMA: Passive reduced-order interconnect macromodeling algorithm," *IEEE Trans. Computer-Aided Design*, vol. 17, pp. 645–654, Aug. 1998.

[5] A. C. Cangellaris and L. Zhao, "Model order reduction techniques for electromagnetic macromodeling based on finite methods," *Int. J. Numer. Modeling, Electron. Networks, Devices, and Fields*, vol. 13, no. 2/3, pp. 181–197, Mar.–June 2000.

[6] Y. Zhu and A. C. Cangellaris, "Finite elements-based model order reduction of electromagnetic devices," *Int. J. Numer. Modeling, Electron. Networks, Devices, and Fields*, vol. 15, no. 1, pp. 73–91, Jan.–Feb. 2002.

[7] D. K. Sun, "ALPS: An adaptive Lanczos–Padè spectral solution of mixed-potential integral equation," *Comput. Methods Appl. Mech. Eng.*, vol. 169, pp. 425–432, 1999.

[8] G. Conciauro, P. Arcioni, and M. Bressan, "Integral equations and state variables in the S-domain modeling of passive multilayered components," in *IEEE MTT-S Int. Microwave Symp. Dig. 2003*, vol. 3, Philadelphia, PA, June 8–13, 2003, pp. 1963–1966.

[9] P. Arcioni, M. Bressan, G. Conciauro, and A. R. Olea Garcia, "Wideband modeling of passive planar components by the BI-RME method," presented at the Eur. Microwave Conf. Workshop, Munich, Germany, Oct. 8, 1999.

[10] ——, "New ideas for frequency/time domain modeling of passive structures for MMICs," presented at the Eur. Congr. on Computational Methods in Applied Sciences and Engineering, Barcelona, Spain, Sept. 11–14, 2000.

[11] P. Arcioni, M. Bressan, and G. Conciauro, "Frequency/time-domain modeling of microstrip circuits by a modified spectral domain approach," in *IEEE MTT-S Int. Microwave Symp. Dig.*, vol. 2, May 20–25, 2001, pp. 1237–1240.

[12] G. V. Eleftheriades and J. R. Mosig, "On the network characterization of planar passive circuits using the method of the moments," *IEEE Trans. Microwave Theory Tech.*, vol. 44, pp. 438–445, Mar. 1996.

[13] A. A. Melcón, J. R. Mosig, and M. Guglielmi, "Efficient CAD of boxed microwave circuits based on arbitrary rectangular elements," *IEEE Trans. Microwave Theory Tech.*, vol. 47, pp. 1045–1058, July 1999.

[14] R. F. Harrington, *Field Computation by Moment Methods*, ser. Electromagn. Waves. Pistacaway, NJ: IEEE Press, 1993.

[15] G. Conciauro and M. Bressan, "Singularity expansion of mode voltages and currents in a layered, anisotropic, dispersive medium included between two ground planes," *IEEE Trans. Microwave Theory Tech.*, vol. 47, pp. 1617–1626, Sept. 1999.
[16] G. H. Golub and C. F. Van Loan, "The singular value decomposition," in *Matrix Computations*, 3rd ed. Baltimore, MD: The Johns Hopkins Univ. Press, 1996, sec. 2.5.3, p. 70, 71, 73.
[17] E. Anderson *et al.*, *LAPACK Users' Guide*, 3rd ed. Philadelphia, PA: SIAM, 1999.
[18] A. W. Glisson and D. R. Wilton, "Simple and efficient numerical methods for problems of electromagnetic radiation and scattering from surfaces," *IEEE Trans. Antennas Propagat.*, vol. AP-28, pp. 593–603, Sept. 1980.
[19] J. P. K. Gilb and C. A. Balanis, "MIS slow-wave structures over a wide range of parameters," *IEEE Trans Microwave Theory Tech.*, vol. 40, pp. 2148–2154, Dec. 1992.
[20] E. Palenczy, D. Kinowski, J. F. Legier, P. Pribetich, and P. Kennis, "Comparison of full wave approaches for determination of microstrip conductor losses for MMIC applications," *Electron. Lett.*, vol. 26, no. 25, pp. 2076–2077, Dec. 1990.
[21] I. S. Gradshtein and I. M. Ryzhik, *Table of Integrals, Series, and Products*, 5th ed. New York: Academic, 1994.

Giuseppe Conciauro (A'72–M'87–SM'03) was born in Palermo, Italy, in 1937. He received the Electrical Engineering and Libera Docenza degrees from the University of Palermo, Palermo, Italy, in 1961 and 1971, respectively.

From 1963 to 1971, he was an Assistant Professor of microwave theory with the Institute of Electrical Engineering, University of Palermo. In 1971, he joined the Department of Electronics, University of Pavia, Pavia, Italy, where he teaches electromagnetic theory as a Full Professor. From 1985 to 1991, he served as Director of the Department of Electronics and, for many years, he chaired the board of the professors of the graduation course in electrical engineering. He currently chairs the Ph.D. school in electronic, electrical engineering and computer science at the University of Pavia. He authored the textbook *Introduzione alle Onde Elettromagnetiche* (Milan, Italy: McGraw-Hill Italia, 1992) and coauthored *Advanced Modal Analysis* (Chichester, U.K.: Wiley, 2000) and *Fondamenti di Onde Elettromagnetiche* (Milan, Italy: McGraw-Hill Italia, 2003). His main research interests are microwave theory, interaction structures for particle accelerators, and numerical methods in electromagnetics.

Prof. Conciauro serves on the Editorial Board of the IEEE TRANSACTIONS ON MICROWAVE THEORY AND TECHNIQUES.

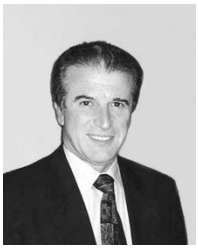

Paolo Arcioni (M'90–SM'03) was born in Busto Arsizio, Italy, in 1949. He received the Laurea degree in electronic engineering from the University of Pavia, Pavia, Italy, in 1973.

In 1974, he joined the Department of Electronics, University of Pavia, where he currently teaches a course in microwave theory as a Full Professor. In 1991, he was a Visiting Scientist with the Stanford Linear Accelerator Center, Stanford, CA, where he has worked in cooperation with the RF Group to design optimized cavities for the PEP II Project. From 1992 to 1993, he collaborated with the Istituto Nazionale de Fisica Nucleare (INFN), Frascati, Italy, with the design of accelerating cavities for the DAΦNE storage ring. His main research interests are in the area of microwave theory, modeling, and design of interaction structures for particle accelerators and development of numerical methods for the electromagnetic computer-aided design of passive microwave components. His current research activities concern the modeling of planar components on semiconductor substrates and of integrated structures for millimeter-wave circuits.

Prof. Arcioni is a member of the Editorial Board of the IEEE TRANSACTIONS ON MICROWAVE THEORY AND TECHNIQUES.

Marco Bressan (M'94) was born in Venice, Italy, in 1949. He received the Laurea degree in electronic engineering from the University of Pavia, Pavia, Italy, in 1972.

Since 1973, he has been with the Department of Electronics, University of Pavia, as a Researcher in electromagnetics. In 1987, he joined the faculty of engineering, University of Pavia, as an Associate Professor. His research interests include analytical and numerical methods to determine electromagnetic fields for the computer-aided design of passive microwave and millimeter-wave components.

Prof. Bressan serves on the Editorial Board of the IEEE TRANSACTIONS ON MICROWAVE THEORY AND TECHNIQUES.